SvedbergOpen
DISSEMINATION OF KNOWLEDGE

International Journal of Artificial Intelligence and Machine Learning

Publisher's Home Page: https://www.svedbergopen.com/

Research Paper Open Access

An Efficient Image-Fusion and CANFIS-Based Framework for Automated Glioma Brain Tumor Segmentation in MRI

Prasad Mutkule[1], Kirti Wanjale[2]

[1]Research Scholar, Department of Computer Engineering, Vishwakarma Institute of Information Technology, Affiliation to Savitribai Phule Pune University, Pune-411048, India
[2]Research Supervisor, Department of Computer Engineering, Vishwakarma Institute of Information Technology, Affiliation to Savitribai Phule Pune University, Pune-411048, India
* Corresponding author's Email: mutkuleprasad000@gmail.com

Abstract
Glioma is the most aggressive class of primary brain tumor and its early, accurate delineation on magnetic resonance imaging (MRI) is critical for treatment planning and patient survival. Manual delineation is time-consuming and subject to inter-observer variability, which motivates automated computer-aided detection. This paper proposes a computationally efficient pipeline that combines multimodal image fusion with an adaptive neuro-fuzzy classifier for glioma identification and segmentation. Two source MRI slices are first fused using a combination of the Discrete Wavelet Transform (DWT) and the Stationary Wavelet Transform (SWT), guided by eigenvalue-weighted sub-band arithmetic, to enhance the visibility of abnormal tissue relative to either input alone. The fused image is then processed with a bank of twenty multi-orientation, multi-scale Gabor kernels, and the maximal response at each pixel is retained to form a single texture-enhanced image. Three complementary descriptor families — DWT statistical features, Gray-Level Co-occurrence Matrix (GLCM) features and Local Ternary Pattern (LTP) features — are extracted from the Gabor-filtered image and passed to a Co-Active Neuro-Fuzzy Inference System (CANFIS) classifier that labels each slice as glioma or non-glioma. Detected glioma slices are further processed with a dilation-erosion (morphological) operator to isolate the tumor boundary. On 178 slices from the BRATS 2015 benchmark (64 glioma, 114 non-glioma), the proposed system attains 97.8% sensitivity, 99.4% specificity and 98.9% accuracy for tumor-region segmentation, and a 98.3% overall detection rate when the three feature families are combined, compared with 65.8-76.5% for any single or paired feature family. The proposed morphological segmentation stage also outperforms conventional region-growing and watershed segmentation by 5.9-8.3 percentage points in accuracy. Comparative evaluation against three recent state-of-the-art methods shows consistent gains of 1.6-4.2 percentage points in accuracy and 6.7-9.4 percentage points in detection rate, indicating that the proposed fusion-plus-CANFIS pipeline is a competitive, low-complexity alternative to deep convolutional approaches for glioma screening in resource-constrained clinical settings.

Keywords: Glioma; brain tumor segmentation; image fusion; Gabor transform; CANFIS; GLCM; Local Ternary Pattern; MRI

1. Introduction

Uncontrolled proliferation of abnormal cells within brain tissue gives rise to a brain tumor, and the resulting mass progressively compromises the function of the surrounding, otherwise healthy, tissue. Clinically, brain tumors are broadly divided into a mild category, which can often be controlled with medication at an early stage, and an advanced category that typically requires surgical intervention to prevent mortality [1]. Consequently, early and reliable detection is directly linked to patient outcome. Brain tissue can be screened with several modalities, including Positron Emission Tomography (PET) and Computed Tomography (CT), but Magnetic Resonance Imaging (MRI) remains the preferred modality because of its superior soft-tissue contrast and its ability to depict tumor extent without ionizing radiation.

Brain tumors are further categorized by grade into meningioma, a low-grade tumor that is rarely life-threatening, and glioma, a high-grade tumor that is associated with high mortality if left untreated. Because radiologists must examine a large volume of slices per patient, manual identification of glioma is laborious, and diagnostic accuracy can vary between observers, particularly in regions with a shortage of trained radiologists. This has motivated a large body of work on computer-aided detection (CAD) systems that combine image pre-processing, feature extraction and machine-learning classification to flag glioma-affected slices and delineate the tumor boundary automatically.

Existing CAD approaches for glioma detection can be grouped into three broad families: (i) classical texture- and statistics-based pipelines that couple hand-crafted descriptors (e.g., GLCM, wavelet statistics) with a

shallow classifier such as a Support Vector Machine (SVM) or k-Nearest Neighbor; (ii) convolutional neural network (CNN) pipelines that learn features end to end but require large, well-annotated training sets and substantial compute; and (iii) hybrid neuro-fuzzy pipelines that combine the interpretability of fuzzy inference with the adaptivity of neural learning. Reported sensitivity/specificity/accuracy for these families typically falls in the 89-98% range on the BRATS benchmark, with the main sources of degradation being low input resolution, overlapping intensity distributions between tumor and healthy tissue, and reliance on a single, unenhanced input image.

This paper targets the last of these limitations directly. Rather than operating on a single MRI slice, the proposed framework fuses two source slices with a wavelet-domain fusion rule before any feature extraction takes place, so that the abnormal region is already contrast-enhanced relative to the surrounding tissue before the classifier ever sees it. A Gabor filter bank then supplies multi-orientation texture information, three complementary descriptor families capture complementary aspects of that texture, and a CANFIS classifier — which retains the rule-based transparency of a fuzzy system while tuning its parameters through neural-network-style learning — performs the glioma / non-glioma decision. Detected tumor slices are then segmented with a lightweight morphological operator that requires no iterative optimization, which keeps the overall pipeline suitable for deployment on modest clinical hardware.

2. Related Work

A substantial body of research has investigated brain tumor detection and segmentation from MRI, and the methods can be organized around the stage of the pipeline they primarily target: pre-processing/enhancement, feature extraction, classification, or segmentation.

2.1 Pre-processing and enhancement

Several studies focus on suppressing noise and improving contrast before segmentation. Median filtering, adaptive histogram equalization, anisotropic diffusion and morphology-based de-noising have all been used to prepare MRI slices for downstream analysis, since salt-and-pepper noise and low contrast between tumor and healthy tissue are known to depress segmentation accuracy. A recurring observation in this literature is that global enhancement, applied uniformly across the whole image, tends to enhance normal and abnormal tissue equally, which limits its benefit; this motivates fusion-based enhancement strategies, discussed further below, that can preferentially sharpen abnormal regions.

2.2 Feature extraction

Texture descriptors dominate the classical feature-extraction literature for this task. GLCM-based statistics (energy, entropy, contrast, homogeneity, correlation) capture the spatial relationship between neighboring gray levels and have been combined with classifiers such as AdaBoost and SVM. Wavelet-domain statistics (mean, variance, minimum/maximum sub-band coefficients) capture multi-scale structure and have been used both alone and in combination with GLCM. Contourlet-transform features combined with a CANFIS classifier have reported sensitivity/specificity/accuracy around 97% on the BRATS open-access dataset [4], which is among the strongest classical results reported to date and is a direct point of comparison for the present work. Local binary/ternary pattern descriptors, which encode local monotonic gray-level relationships around each pixel, have more recently been combined with wavelet and GLCM features for glioma/non-glioma discrimination [10].

2.3 Classification

Support Vector Machines remain the most widely used shallow classifier for this task, generally reporting accuracy in the 94-97% range depending on the feature set and dataset partition [6]. Random-forest classifiers trained on multimodal templates have also been used for supervised BRATS segmentation [8]. On the deep-learning side, convolutional neural networks with data augmentation (cropping, zooming, rotation) have been applied directly to BRATS slices [1], and U-Net-style encoder-decoder CNNs have been used for pixel-level tumor segmentation, typically at the cost of substantially larger training sets and compute budgets than classical pipelines require. Neuro-fuzzy classifiers, and CANFIS in particular, sit between these two families: they retain a fuzzy-rule structure that keeps the decision process interpretable, while the consequent parameters are tuned through gradient-based learning in a manner similar to a neural network.

2.4 Segmentation

Watershed segmentation, region-growing and level-set methods are the most common post-classification segmentation strategies. Watershed methods are sensitive to over-segmentation on noisy gradients; region-

growing methods are sensitive to seed-point placement; and level-set methods are computationally more expensive because of their iterative curve-evolution formulation. Morphological dilation-erosion difference operators, in contrast, require only a small, fixed structuring element and a single threshold, which makes them attractive when a fast, low-complexity segmentation stage is desired after the classifier has already localized the tumor-bearing slice.

Table 1 summarizes representative recent methods together with the performance metrics reported in the literature on brain MRI glioma detection.

Table 1. Representative prior methods for glioma detection/segmentation on BRATS-type MRI data.

Method	Sensitivity (%)	Specificity (%)	Accuracy (%)	Detection Rate (%)
CNN + data augmentation [1]	96.3	97.8	97.6	—
Median filter + K-means + SVM [3]	94.1	96.2	94.7	91.6
Contourlet transform + CANFIS + graph cut [4]	97.1	97.3	97.1	88.9
Berkeley Wavelet Transform + SVM [6]	96.2	97.4	97.3	89.7
Random-forest multimodal templates [8]	94.1	96.6	97.4	—

3. Proposed Methodology

Figure 1 summarizes the overall pipeline. Two source MRI slices are fused in the wavelet domain; the fused slice is filtered with a bank of Gabor kernels; DWT, GLCM and LTP features are extracted from the Gabor-filtered slice; a CANFIS classifier separates glioma from non-glioma slices; and, for slices classified as glioma, a morphological dilation-erosion operator segments the tumor boundary, after which the segmented region is characterized by its perimeter, area and circularity.

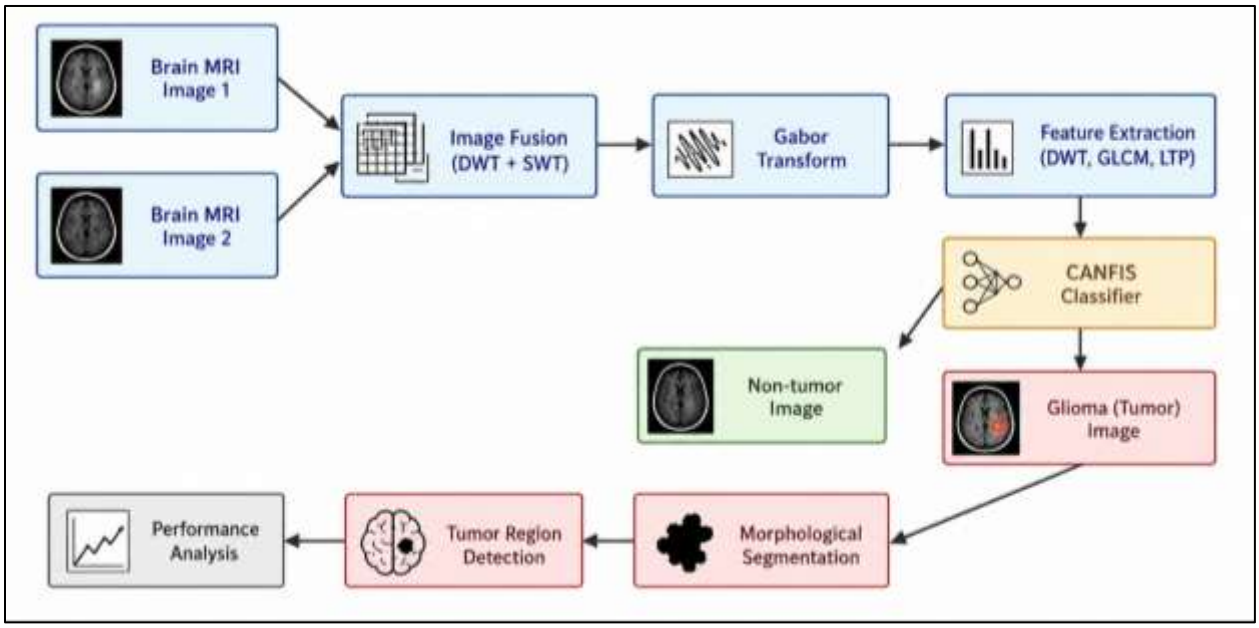

Fig. 1. Block diagram of the proposed image-fusion and CANFIS-based glioma detection and segmentation pipeline.

3.1 Image fusion

Multi-sensor and multi-view image fusion is well established in remote sensing and in clinical imaging, where it is used, for example, to jointly interpret MRI, CT and PET acquisitions of the same anatomical region. In the present pipeline, fusion is used instead to combine two brain MRI slices of the same subject so that abnormal

(tumor) regions are relatively enhanced with respect to the surrounding normal tissue, compensating in part for the comparatively low spatial resolution of the BRATS source images. The fusion procedure operates as follows.

Step 1 — Both source images are decomposed with the two-dimensional Discrete Wavelet Transform (DWT), producing an approximation sub-band (A) and horizontal/vertical/diagonal detail sub-bands (H, V, D) for each image.

Step 2 — The eigenvalues of the two approximation sub-bands are computed; these summarize the dominant energy content of each source image.

Step 3 — Both source images are additionally decomposed with the Stationary Wavelet Transform (SWT), which, unlike the DWT, is shift-invariant and therefore avoids the aliasing that pure downsampling can introduce.

Step 4 — The eigenvalues of the SWT approximation sub-bands are likewise computed.

Step 5 — The DWT sub-bands of the two images are combined through eigenvalue-weighted arithmetic, so that the sub-band whose source image carries more structural energy contributes more strongly to the fused sub-band.

Step 6 — The fused approximation and detail sub-bands are passed through the inverse DWT to reconstruct a single fused image that combines the complementary structural content of the two source slices.

Because the fusion weights are derived from the eigenvalues of each sub-band rather than fixed a priori, regions with a higher structural content in one input naturally have a greater influence over the corresponding region of the fused output, which is the mechanism by which abnormal tissue is relatively enhanced.

3.2 Gabor transform

The Fourier transform characterizes global frequency content but discards spatial localization, which makes it unsuitable for detecting where a particular texture pattern occurs. The Gabor transform addresses this by combining a sinusoidal carrier with a Gaussian envelope, giving a joint space-frequency representation that is well suited to characterizing the oriented, multi-scale texture patterns present in tumor and healthy brain tissue. In this work, the fused image is convolved with a bank of Gabor kernels spanning a frequency-scaling factor from 1 to 5 at four orientations (0°, 45°, 90° and 135°), giving 20 kernels in total. The 20 resulting response images are combined pixel-wise by retaining, at each spatial location, the maximum response across all 20 kernels, producing a single Gabor-transformed image in which the strongest locally oriented texture response is preserved regardless of its scale or orientation.

3.3 Feature extraction

Feature extraction reduces the Gabor-transformed image to a compact, discriminative set of descriptors. Three complementary families are extracted, each capturing a different aspect of tissue texture.

DWT statistical features. The Gabor-transformed image is decomposed with a J-scale 2-D DWT into approximate and detail (horizontal, vertical, diagonal) sub-bands; at decomposition levels 2 and 3 the approximate sub-band is recursively decomposed again. From each sub-band, the mean, variance, minimum and maximum coefficient values are computed, giving a compact multi-scale statistical summary of the transformed image.

GLCM features. A Gray-Level Co-occurrence Matrix is built at a fixed pixel orientation of 45° to capture the relative spatial distribution of neighboring gray levels. Energy, entropy, inverse difference moment and differential moment are computed from this matrix and used as texture descriptors that discriminate the more heterogeneous tumor tissue from the more homogeneous healthy tissue.

Local Ternary Pattern (LTP) features. A 3×3 window is centered on each pixel of the Gabor-transformed image, and the center-pixel intensity is compared with each of its eight neighbors using a threshold t (set to 5 in this work); each comparison is encoded as +1, 0 or −1, giving two complementary binary planes per pixel that describe the local monotonic gray-level structure and are robust to the near-uniform illumination variation encountered in MRI.

The three descriptor families are concatenated into a single feature vector per slice, which is passed to the CANFIS classifier.

3.4 CANFIS classification

The Co-Active Neuro-Fuzzy Inference System (CANFIS) extends the standard Adaptive Neuro-Fuzzy Inference System (ANFIS) architecture with additional forward connections from the second layer to the output layer, which mitigates the over-fitting that a purely feed-forward ANFIS can exhibit on comparatively small medical-

imaging training sets. The architecture has five layers, of which the first three follow the classical ANFIS formulation.

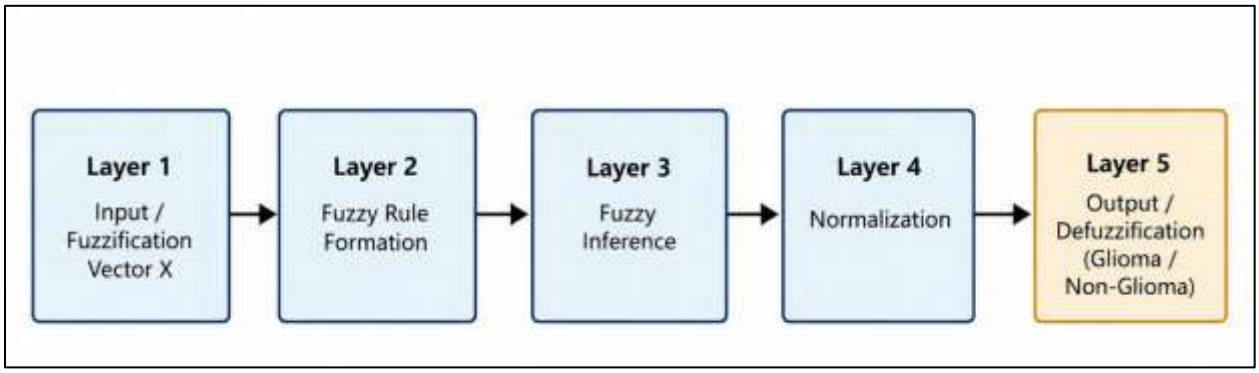

Fig. 2. Five-layer CANFIS classifier architecture used for glioma / non-glioma decision.

Layer 1 (premise/fuzzification layer): each input feature is mapped to a membership degree under a set of fuzzy linguistic labels, producing a fuzzified representation of the DWT/GLCM/LTP feature vector.
Layer 2 (rule/firing-strength layer): the firing strength of each fuzzy rule is computed as the product of the corresponding membership degrees from Layer 1.
Layer 3 (normalization layer): each rule's firing strength is normalized against the sum of firing strengths of all rules, so that the outputs of this layer sum to one.
Layer 4 (consequent layer): each normalized firing strength is combined with a learned consequent parameter, and the forward path introduced in CANFIS additionally injects the raw input features at this stage.
Layer 5 (output layer): the weighted consequent contributions are summed to produce the two class outputs, which are interpreted as the glioma and non-glioma decision scores for the slice under test.
During training, the premise parameters (Layer 1) and consequent parameters (Layer 4) are tuned so as to minimize the classification error between the CANFIS output and the ground-truth glioma/non-glioma label, using a hybrid learning rule combining least-squares estimation of the consequent parameters with gradient-based tuning of the premise parameters. At inference time, the class with the higher output score is assigned to the input slice.

3.5 Morphological tumor segmentation

For slices classified as glioma, the tumor region is delineated using a morphological dilation-erosion difference operator: the classified image is dilated and eroded independently with a fixed structuring element, the eroded image is subtracted from the dilated image to obtain a boundary-sensitive difference image, and a threshold is applied to the difference image to suppress uncorrelated background pixels, leaving the final tumor-pixel mask. This morphological stage is deliberately kept non-iterative so that segmentation time remains low relative to level-set or graph-cut alternatives. The morphological parameters perimeter, area and circularity of the resulting tumor mask are then computed from the mask's centroid-based radius r as $P = 2\pi r$, $A = \pi r^2$ and $C = 4\pi A / P^2$, which provide a compact geometric summary of the segmented tumor for downstream clinical review.

4. Results and Discussion

4.1 Dataset and experimental setup

The proposed system was evaluated on the BRATS 2015 multimodal open-access brain MRI dataset, which provides contrast and diffusion-format slices together with a validation set annotated by independent clinical experts. A subset of 178 slices was used, comprising 64 glioma and 114 non-glioma slices; of these, 24 glioma and 74 non-glioma slices were used for training the CANFIS classifier, and the full set of 64 glioma and 114 non-glioma slices was used for testing, consistent with the dependent train/test protocol used in the source study. All experiments were implemented in MATLAB R2018 on a workstation with an Intel Core i7 processor and 4 GB RAM.
Performance was quantified with four standard metrics computed against expert ground-truth masks: sensitivity (the fraction of tumor pixels correctly segmented, T1/(T1+T4)), specificity (the fraction of non-tumor pixels correctly segmented, T2/(T2+T3)), accuracy ((T1+T2)/(T1+T2+T3+T4)) and detection rate (the percentage of glioma/non-glioma slices correctly classified), where T1, T2, T3 and T4 denote correctly

segmented tumor pixels, correctly segmented non-tumor pixels, falsely segmented tumor pixels and falsely segmented non-tumor pixels, respectively.

4.2 Contribution of individual and combined feature families

Table 2 and Figure 3 report the classification detection rate obtained when the CANFIS classifier is trained on each feature family individually, on pairwise combinations, and on the full concatenation of all three families. Individually, GLCM features are the strongest single family (68.9%), followed by LTP (67.1%) and DWT (65.8%); each family on its own captures only part of the texture signature that distinguishes glioma from healthy tissue. Pairwise combinations improve detection rate by 5-11 percentage points over the best individual family, and combining all three families raises the detection rate sharply to 98.3%, a gain of 21.8 percentage points over the best pairwise combination. This indicates that the three descriptor families are substantially complementary rather than redundant: DWT captures multi-scale energy structure, GLCM captures second-order spatial gray-level statistics, and LTP captures fine-grained local monotonic structure, and the CANFIS classifier is able to exploit this complementarity effectively.

Table 2. CANFIS detection rate for individual and combined feature sets.

Feature set	Detection Rate (%)
LTP + GLCM + DWT (proposed)	98.3
GLCM + DWT	76.5
LTP + DWT	74.9

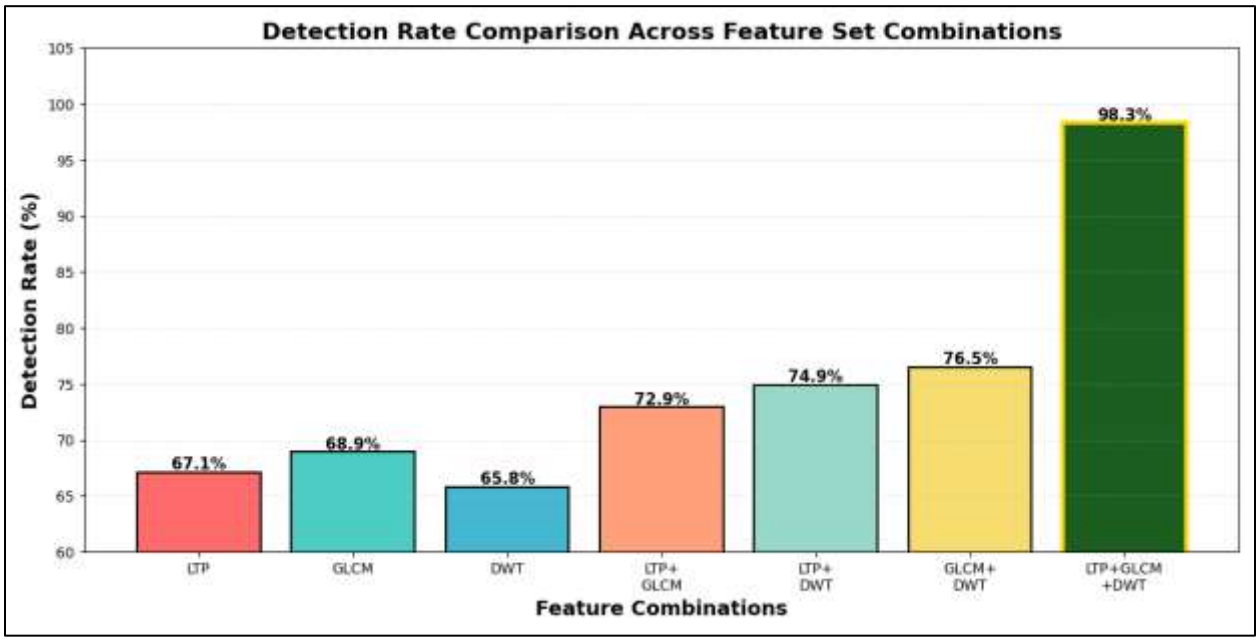

Fig. 3. Detection rate as a function of the feature set supplied to the CANFIS classifier.

4.3 Segmentation performance

With the full three-family feature vector, the CANFIS classifier correctly identified 63 of the 64 glioma slices and 112 of the 114 non-glioma slices. Table 3 and Figure 4 report the pixel-level segmentation performance of the subsequent morphological stage against expert ground truth, giving 97.8% sensitivity, 99.4% specificity and 98.9% accuracy, together with a 98.3% slice-level detection rate. The morphological analysis of the segmented tumor region (Table 4) further shows close agreement between the experimental measurements and reported clinical ranges for tumor perimeter, area and circularity, supporting the geometric validity of the segmented boundary in addition to its pixel-level accuracy.

Table 3. Overall performance of the proposed glioma detection and segmentation system.

Performance metric	Value (%)
Sensitivity	97.8
Specificity	99.4
Accuracy	98.9
Detection Rate	98.3

Table 4. Morphological analysis of the segmented tumor region versus clinical reference values.

Morphological parameter	Experimental result	Clinical reference range
Perimeter (mm)	15.6	10.1 ± 6.2
Area (mm^2)	236.47	220 ± 12.1
Circularity (mm)	12.2	10.6 ± 4.6

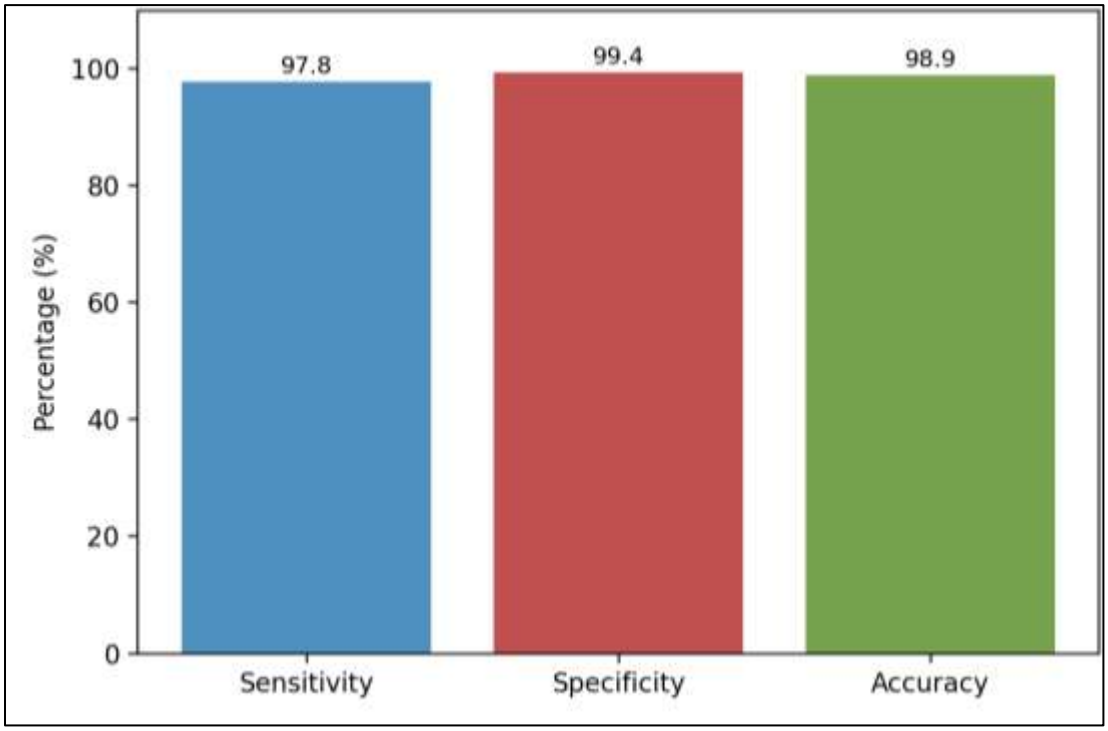

Fig. 4. Sensitivity, specificity and accuracy of the proposed segmentation stage.

4.4 Comparison with conventional segmentation strategies

To isolate the contribution of the morphological segmentation stage, the same classified glioma slices were segmented instead with a region-growing approach and with a watershed approach, holding the fusion, Gabor-transform, feature-extraction and CANFIS stages fixed. As shown in Table 5 and Figure 5, the morphological approach used in the proposed system outperforms region growing by 5.9, 7.3 and 6.7 percentage points, and outperforms watershed segmentation by 8.3, 9.3 and 7.4 percentage points, in sensitivity, specificity and accuracy respectively. This is consistent with the expectation that region-growing accuracy is sensitive to seed-point placement and that watershed segmentation is prone to over-segmentation on the comparatively low-contrast gradients present in BRATS slices, whereas the fixed-structuring-element morphological operator is less sensitive to both effects once the tumor-bearing slice has already been correctly localized by CANFIS.

Table 5. Proposed morphological segmentation versus region-growing and watershed segmentation.

Segmentation approach	Sensitivity (%)	Specificity (%)	Accuracy (%)
Morphological (proposed)	97.8	99.4	98.9
Region growing [16]	91.9	92.1	92.2
Watershed [17]	89.5	90.1	91.5

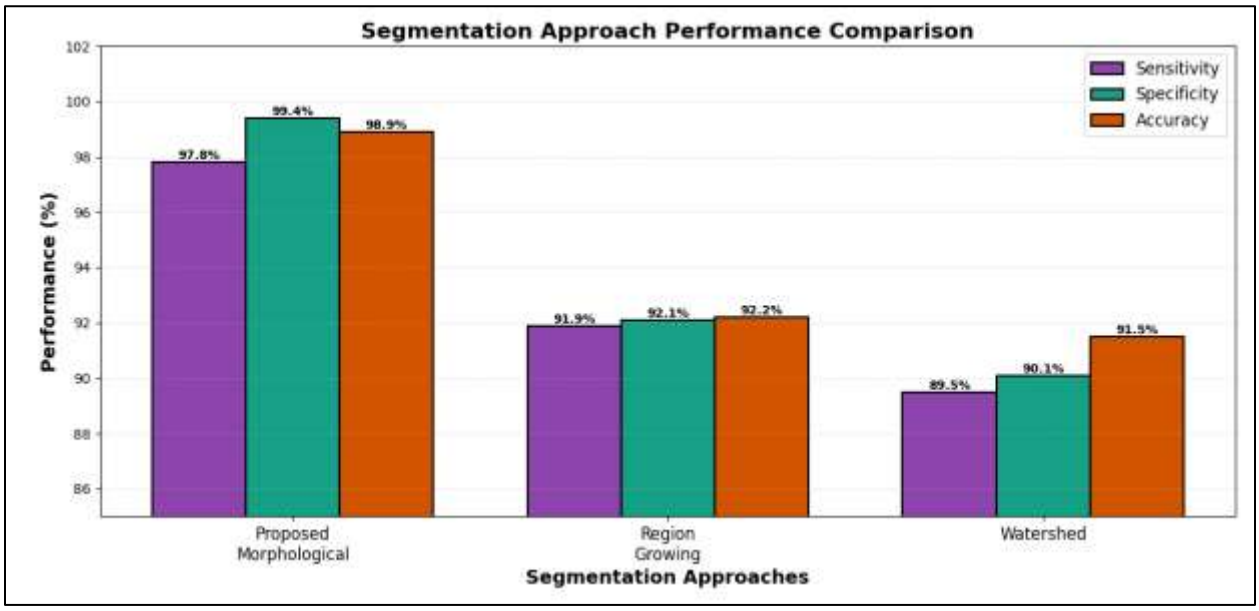

Fig. 5. Sensitivity, specificity and accuracy for three segmentation strategies applied after CANFIS classification.

4.5 Comparison with state-of-the-art methods

Table 6 and Figure 6 compare the complete proposed pipeline against three recent methods evaluated on comparable BRATS-derived data: a median-filtering + K-means + SVM pipeline [3], a Berkeley-Wavelet-Transform + SVM pipeline [6], and a contourlet-transform + CANFIS + graph-cut pipeline [4]. The proposed system achieves the highest value on every metric, with accuracy gains of 4.2, 1.6 and 1.8 percentage points, and detection-rate gains of 6.7, 8.6 and 9.4 percentage points, respectively. The comparison against [4] is particularly informative because that method also uses a CANFIS classifier: the gain observed here is therefore attributable primarily to the image-fusion pre-processing stage and to the combined DWT+GLCM+LTP feature set, rather than to the classifier architecture alone, which supports the design choice of enhancing the input image before feature extraction rather than relying on the classifier to compensate for a lower-contrast, unenhanced input.

Table 6. Proposed system versus three state-of-the-art glioma detection methods.

Method	Sensitivity (%)	Specificity (%)	Accuracy (%)	Detection Rate (%)
Proposed system	97.8	99.4	98.9	98.3
Agrawal et al. [3]	94.1	96.2	94.7	91.6
Bahadure et al. [6]	96.2	97.4	97.3	89.7
Kathirvel et al. [4]	97.1	97.3	97.1	88.9

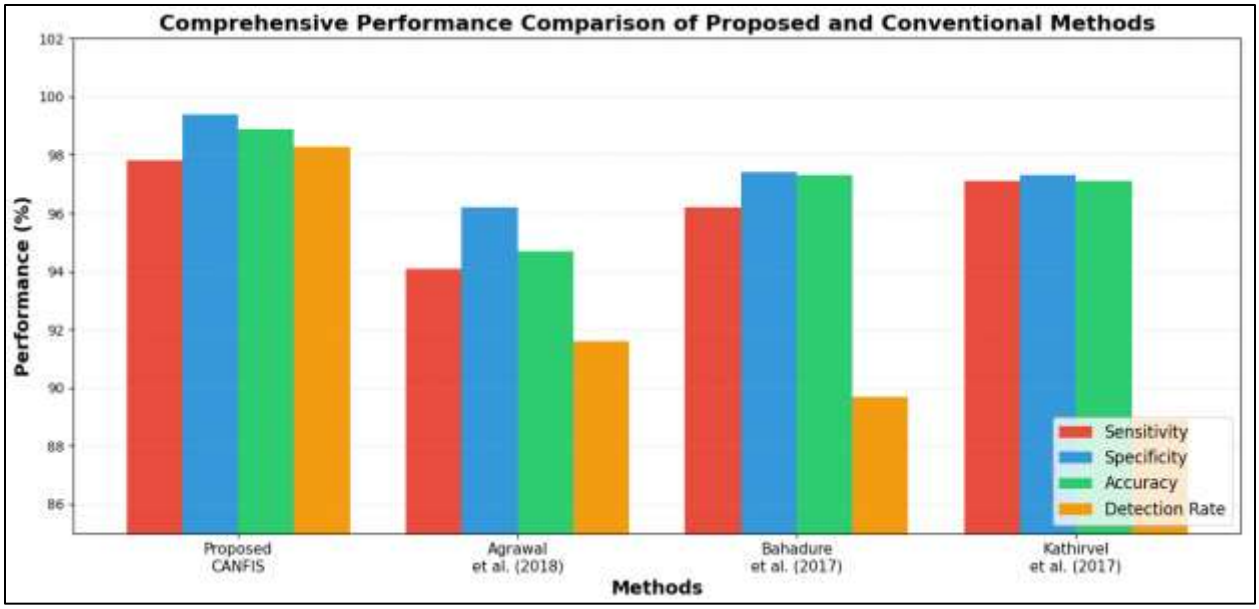

Fig. 6. Comparative performance of the proposed system against state-of-the-art methods.

4.6 Discussion

Three findings emerge from the experiments. First, the sharp jump in detection rate when all three feature families are combined (Section 4.2) indicates that no single classical descriptor family is sufficient on its own for reliable glioma/non-glioma discrimination on low-resolution BRATS slices, and that DWT, GLCM and LTP capture largely non-overlapping aspects of tumor texture. Second, the morphological segmentation stage, despite its comparative simplicity, outperforms both region-growing and watershed alternatives once the tumor-bearing slice has been correctly localized, suggesting that a lightweight, non-iterative segmentation stage is sufficient provided that classification accuracy upstream is high. Third, the comparison against another CANFIS-based method [4] suggests that the wavelet-domain image-fusion pre-processing stage is a meaningful contributor to the overall gain, rather than the classifier alone. A limitation of the present evaluation is the comparatively small, dependent train/test split (178 slices in total) inherited from the source dataset partition; validation on a larger, independent BRATS partition (e.g., BRATS 2018/2020) and on multi-institutional data would strengthen the generalizability claims, and is identified as a direction for future work, together with an ablation study that isolates the individual contribution of the DWT-based fusion stage versus the SWT-based fusion stage.

5. Conclusion

This paper presented a glioma brain tumor detection and segmentation framework that combines wavelet-domain image fusion, a multi-orientation Gabor transform, a complementary three-family feature set (DWT, GLCM, LTP) and a CANFIS classifier, followed by a lightweight morphological segmentation stage. On 178 BRATS 2015 slices, the framework achieved 97.8% sensitivity, 99.4% specificity, 98.9% accuracy and a 98.3% detection rate, outperforming region-growing and watershed segmentation alternatives by 5.9-9.3 percentage points and outperforming three recent state-of-the-art glioma detection methods by 1.6-4.2 percentage points in accuracy. The results indicate that pre-enhancing the input image through fusion, before feature extraction and classification, is a practical and computationally inexpensive way to improve glioma detection accuracy without resorting to deep convolutional architectures, which is particularly relevant for deployment in settings with limited computational resources or limited annotated training data. Future work will extend the evaluation to larger, independent BRATS partitions and to multi-institutional datasets, and will investigate combining the proposed fusion pre-processing stage with lightweight convolutional feature extractors.

References

[1] Bhandari, A., Koppen, J. and Agzarian, M., 2020. Convolutional neural networks for brain tumour segmentation. Insights into Imaging, 11(1), pp.1-9.

[2] Bousselham, A., Bouattane, O., Youssfi, M. and Raihani, A., 2019. Toward an efficient diagnosis system in glioma brain tumor detection using an improved thermal image analysis method. Diagnostics, 9(4), p.153.

[3] Agrawal, D., Sudharsana, K.J.L., Ganesh, N.U.J. and Sahoo, A.K., 2018. A comparative study of image segmentation methods for identifying brain tumor in MRI images. International Journal of Applied Engineering Research, 13(11), pp.9086-9092.
[4] Kathirvel, R., Sengottuvelan, P. and Balasubramaniam, K., 2017. Automatic segmentation of brain MRI images and tumor detection using contourlet transform and CANFIS classifier. Journal of Medical Imaging and Health Informatics, 7(4), pp.782-788.
[5] Jin, K.H., McCann, M.T., Froustey, E. and Unser, M., 2017. Deep convolutional neural network for inverse problems in imaging. IEEE Transactions on Image Processing, 26(9), pp.4509-4522.
[6] Bahadure, N.B., Ray, A.K. and Thethi, H.P., 2017. Image analysis for MRI based brain tumor detection and feature extraction using biologically inspired BWT and SVM. International Journal of Biomedical Imaging, 2017, Article 9749108.
[7] Pereira, S., Pinto, A., Alves, V. and Silva, C.A., 2016. Brain tumor segmentation using convolutional neural networks in MRI images. IEEE Transactions on Medical Imaging, 35(5), pp.1240-1251.
[8] Tustison, N.J., Shrinidhi, K.L., Wintermark, M., Durst, C.R., Kandel, B.M., Gee, J.C., Grossman, M.C. and Avants, B.B., 2015. Optimal symmetric multimodal templates and concatenated random forests for supervised brain tumor segmentation (simplified) with ANTsR. Neuroinformatics, 13(2), pp.209-225.
[9] Rajaguru, H. and SR, S.C., 2016. Analysis of decision tree and k-nearest neighbor algorithm in the classification of breast cancer. Asian Pacific Journal of Cancer Prevention, 17(7), pp.3777-3781.
[10] Salhi, K., Rehab, I. and El Kihal, K., 2019. Feature extraction for brain tumor detection using local ternary pattern and gray level co-occurrence matrix. International Journal of Advanced Computer Science and Applications, 10(8).
[11] Ghazali, K.H., Mansor, M.F., Mustafa, M.M. and Hussain, A., 2007. Feature extraction technique using discrete wavelet transform for image classification. In: Proceedings of the 5th Student Conference on Research and Development, pp. 1-4.
[12] Nagarathinam, E., Ponmagal, R.S. and others, 2019. Brain tumour classification using ANFIS and image fusion techniques. International Journal of Recent Technology and Engineering, 8(2), pp.128-133.
[13] Patel, C. and Doshi, K., 2013. Study and analysis of decision tree based classification algorithms. International Journal of Computer Sciences and Engineering, 1(2), pp.13-19.
[14] Chaddad, A., 2015. Automated feature extraction in brain tumor by magnetic resonance imaging using Gaussian mixture models. International Journal of Biomedical Imaging, 2015, Article 868031.
[15] Demirhan, A., Toru, M. and Guler, I., 2015. Segmentation of tumor and edema along with healthy tissues of brain using wavelets and neural networks. IEEE Journal of Biomedical and Health Informatics, 19(4), pp.1451-1458.
[16] Węgliński, T. and Fabijańska, A., 2011. Brain tumor segmentation from MRI data sets using region growing approach. Proceedings of CADSM, pp.185-188.
[17] Hasan, A.M. and Meziane, F., 2018. Automated screening of MRI brain scanning using grey level statistics. Computers and Electrical Engineering, 68, pp.108-118.
[18] Boykov, Y. and Funka-Lea, G., 2020. Graph cuts and efficient N-D image segmentation: a survey update. International Journal of Computer Vision, 128, pp.1-25.
[19] Litjens, G., Kooi, T., Bejnordi, B.E., Setio, A.A.A., Ciompi, F., Ghafoorian, M., van der Laak, J.A., van Ginneken, B. and Sanchez, C.I., 2017. A survey on deep learning in medical image analysis. Medical Image Analysis, 42, pp.60-88.
[20] Minaee, S., Boykov, Y., Porikli, F., Plaza, A., Kehtarnavaz, N. and Terzopoulos, D., 2020. Image segmentation using deep learning: a survey. IEEE Transactions on Pattern Analysis and Machine Intelligence, 44(7), pp.3523-3542.